

# Dimensional and doping stability of Peierls charge density waves

Aitor Garcia-Ruiz (艾飛宇),<sup>1,\*</sup> Che-pin Hsu (許哲彬),<sup>1</sup> Ming-Hao Liu (劉明豪),<sup>1</sup> and Marcin Mucha-Kruczynski<sup>2,†</sup>

<sup>1</sup>*Department of Physics and Center for Quantum Frontiers of Research and Technology (QFort),  
National Cheng Kung University, Tainan 70101, Taiwan*

<sup>2</sup>*Department of Physics, University of Bath, Claverton Down, Bath, BA2 7AY, United Kingdom*

The Peierls instability, the spontaneous dimerization of a one-dimensional metallic chain at half filling, is a paradigmatic mechanism for charge-density-wave (CDW) formation. Here we test its robustness under finite doping and interchain hybridization in finite-thickness arrays of identical chains. We find that the stacking geometry plays a decisive role in stabilizing CDW order away from half filling. In particular, parallel-coupled chains exhibit a bistable regime where the normal and dimerized states coexist as local minima of the total energy, while skew-coupled chains display reentrant CDW order upon doping. Our results demonstrate that even minimal models of coupled atomic chains host rich phase diagrams controlled by doping, lattice rigidity, and interchain coupling geometry.

## I. INTRODUCTION

Low-dimensional materials host an exceptional variety of correlated electronic phases driven by electron-electron interactions [1–8], disorder [9–14] and electron-phonon coupling [15–19]. Among the most prominent, are charge density waves (CDWs), characterised by a periodic modulation of the electronic density accompanied by a lattice distortion [20–27]. In layered transition-metal dichalcogenides (TMDs) [28–30] and related compounds [31, 32], CDWs are ubiquitous and often appear in close proximity to superconductivity and other broken symmetry states. Many materials exhibit several competing CDW orders or different lattice distortion patterns for the same CDW periodicity that lie close in energy [33, 34], leading to metastability [35–37], hysteretic behaviour [38, 39] and bistable switching [40, 41]. While weak-coupling pictures frequently motivate CDW formation in terms of the Peierls mechanism of Fermi surface nesting and enhanced charge susceptibility at a characteristic wave vector, the observed complexity is often attributed to material-specific ingredients such as multi-orbital physics, strong coupling to the lattice and long-range interactions [21, 28].

Peierls pointed out that, in one dimension, a lattice distortion of a half filled chain with wave vector  $2k_F$  opens a gap at the Fermi points, lowering the electronic energy and rendering the metallic state unstable [42]. Equivalently, the static charge susceptibility diverges at  $2k_F$ , making the Peierls instability essentially unavoidable. However, this nesting-based picture is strongly tied to the kinematics of a 1D Fermi surface and generally loses predictive power in higher dimensions in the presence of more complex Fermi surfaces so that peaks in the charge susceptibility do not necessarily determine a unique ordering wave vector or CDW pattern [21]. Nevertheless, the Peierls mechanism provides a minimal and intuitive framework for studying CDW formation and it remains an important open question how much of the observed phenomenology can already emerge from minimal microscopic models.

Here, we study the fate of the Peierls mechanism in arrays

of coupled atomic chains, scenario which allows us to explore the impact of another spatial dimension. Interchain hybridization discretizes the transverse motion into a set of subbands so that even weak coupling produces multiple Fermi crossings. As a result, small changes in doping can move the chemical potential across several band crossings and the CDW instability is no longer governed by a single  $2k_F$  condition of an isolated chain. Instead, it depends sensitively on the subband structure and on which crossings can be gapped by the lattice distortion. Crucially, this is controlled by the stacking geometry, which determines which degeneracies are protected by symmetry and which are lifted by hybridization. For parallel stacking of chains, we find a bistable regime in which the normal and CDW states coexist as distinct local minima of the total energy. For skew stacking, we identify reentrant CDW order upon doping. Our results demonstrate that coupled atomic chains provide a remarkably simple platform in which interchain hybridization and geometry alone generate CDW competition and metastability, offering an intuitive route towards complex phenomenology within a minimal framework.

## II. 1D CHAIN UNDER DOPING: PEIERLS MECHANISM

We start from discussing an infinite one-dimensional chain of single-orbital atoms, distanced  $a$  apart, half filled with spinless electrons. Electrons hop between nearest-neighbor sites with bare amplitude  $t$ . We investigate the Peierls instability towards a dimerized ground state, in which alternating bonds are shortened and elongated by a static displacement  $x$ , as illustrated in the insets of Fig. 1(b). The lattice is modeled by harmonic bonds, so that a distortion costs an elastic energy  $Kx^2/2$  per bond, where  $K$  is the spring constant. The modulation of the bond length is accompanied by a modulation of the hopping amplitude, which we parameterize as  $\delta \equiv \Delta t = -\alpha x$ , with  $\alpha$  the electron-lattice coupling constant. The resulting electronic Hamiltonian is that of an infinite Su-Schrieffer-Heeger (SSH) chain [43]. Using the sublattice amplitude basis,  $\{\psi^A, \psi^B\}$ , where  $A$  and  $B$  denote the sites in the unit cell of length  $2a$ , the Hamiltonian reads,

$$H_k = \begin{pmatrix} 0 & f_k \\ f_k^* & 0 \end{pmatrix}, \quad f_k \equiv t_- + t_+ e^{i2ak}, \quad (1)$$

\* aitor.garcia-ruiz@phys.ncku.edu.tw

† m1mk20@bath.ac.uk

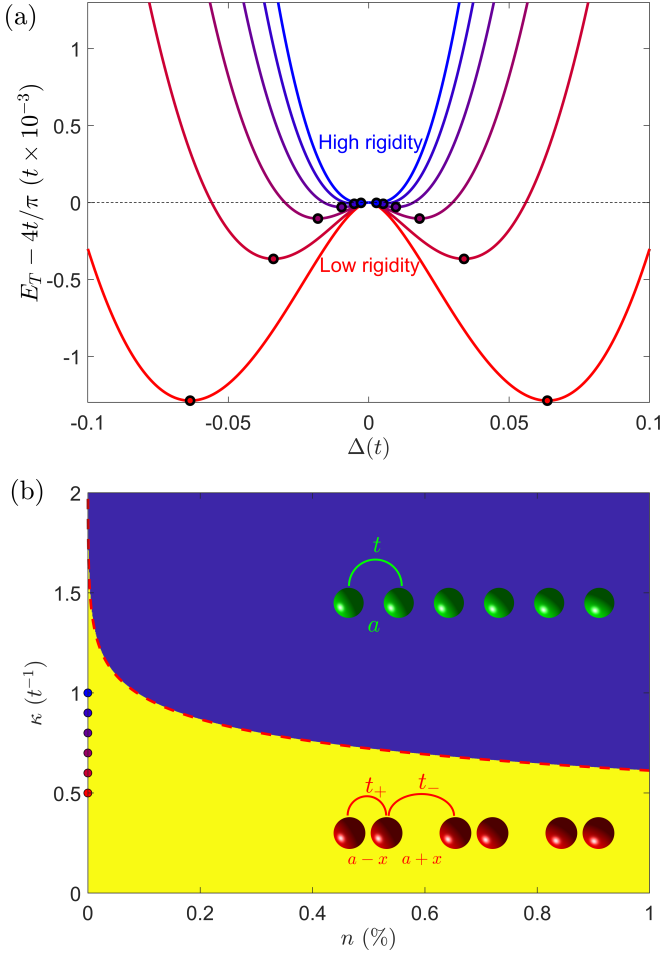


FIG. 1. (a) Total energy curves for six different values of  $\kappa$  between  $\kappa = 0.5t^{-1}$  and  $\kappa = t^{-1}$ . Dots represent the position of the global minima of each curve, computed using Eq. (4). (b) Phase diagram where the normal (blue) and the Peierls CDW order (yellow) regions are separated by a red dashed curve given analytically in Eq. (6). The inset shows the two structural configuration we considered in this work.

where  $t_{\pm} = t \pm \delta/2$  and  $2a$  is the unit cell length. The band energies are  $\epsilon_{\beta}(k) = \beta|f_k|$  ( $\beta = \pm 1$ ), and determine the electronic contribution to the total energy. Equivalently, this static SSH description can be obtained from the zero-temperature electron-phonon Hamiltonian after a unitary transformation (see Appendix A). Including the elastic energy, the total energy per unit cell takes the form

$$E_{\text{T}} = 4t^2\kappa\Delta^2 - \frac{4ta}{\pi} \int_0^{k_{\text{F}}} \sqrt{1 - (1 - \Delta^2) \sin^2(ak)} dk, \quad (2)$$

where we introduce the dimensionless order parameter  $\Delta = \delta/2t$  and rigidity  $\kappa = K/\alpha^2$  for compactness, and  $k_{\text{F}}$  is the Fermi wavelength, which encodes the filling. Owing to electron-hole symmetry about half filling, Eq. (2) applies equally to electron and hole doping.

At half filling,  $k_{\text{F}} = \pi/2a$ , and the electronic contribution reduces to the complete elliptic integral of the second

kind [44, 45], with modulus  $\sqrt{1 + \Delta^2}$ . Expanding Eq. (2) for  $|\Delta| \ll 1$ , we obtain

$$E_{\text{T}}^{\text{HF}} \approx 4t^2\kappa\Delta^2 - \frac{4t}{\pi} \left\{ 1 + \frac{1}{2} \left[ \ln\left(\frac{4}{\Delta}\right) - \frac{1}{2} \right] \Delta^2 \right\}. \quad (3)$$

Minimizing this expression yields the optimal order parameter (see appendix B),

$$\Delta_0 = \pm \frac{4}{e} e^{-2\pi t \kappa}. \quad (4)$$

Importantly,  $\Delta_0$  remains nonzero for any finite rigidity  $\kappa$ , reflecting the Peierls instability of a one-dimensional metal at half filling [42]. The corresponding minima are indicated by dots in the energy profiles of Fig. 1(a).

Away from half filling, Eq. (2) can be expressed in terms of incomplete elliptic integrals (see Appendix C). Writing  $k_{\text{F}} = \pi/2a - \epsilon/a$  ( $\epsilon$  is a dimensionless measure of the doping), Eq. (2) becomes

$$E_{\text{T}} = 4t^2\kappa\Delta^2 - \frac{4t}{\pi} \int_0^{\frac{\pi}{2}-\epsilon} \sqrt{1 - (1 - \Delta^2) \sin^2(\phi)} d\phi \quad (5)$$

$$\approx E_{\text{T}}^{\text{HF}} + \frac{2t}{\pi} \left[ \epsilon \sqrt{\epsilon^2 + \Delta^2} + \Delta^2 \ln \left( \frac{\epsilon + \sqrt{\epsilon^2 + \Delta^2}}{\Delta} \right) \right].$$

For  $\epsilon \neq 0$ , the additional logarithmic term regularizes the  $\Delta \rightarrow 0$  behavior of the half filled energy functional, so that  $\Delta = 0$  is no longer necessarily unstable. The stability of the normal state is determined by the curvature at  $\Delta = 0$ . Requiring  $\partial^2 E_{\text{T}} / \partial \Delta^2|_{\Delta=0} > 0$  yields the exact condition,

$$-2t\pi\kappa < \ln \left[ \tan \left( \frac{\epsilon}{2} \right) \right] + \cos \epsilon, \quad (6)$$

which defines the phase boundary between the dimerized (Peierls) state and the normal state in Fig. 1(b), where the doping  $n$  is expressed as the percentage of excess electron density relative to half filling. Note that we restrict our analysis to low doping, where Fermi-surface nesting does not induce CDW orders with different periodicity.

### III. 1D COUPLED CHAINS

For an array of  $N$  identical, weakly-coupled chains, the Hamiltonian, in the basis of orbital amplitude  $\Psi^{\dagger} = \{\psi_1^{A\dagger}, \psi_1^{B\dagger}, \dots, \psi_N^{A\dagger}, \psi_N^{B\dagger}\}$ , takes the block-tridiagonal form

$$\mathcal{H} = \begin{pmatrix} H_k & T_{1,2} & 0 & \cdots & 0 \\ T_{1,2}^{\dagger} & H_k & T_{2,3} & \cdots & 0 \\ 0 & T_{2,3}^{\dagger} & H_k & \cdots & 0 \\ \vdots & \vdots & \vdots & \ddots & \vdots \\ 0 & 0 & 0 & \cdots & H_k \end{pmatrix}. \quad (7)$$

Above, the diagonal  $2 \times 2$  blocks  $H_k$  describe a single chain and the off-diagonal blocks  $T_{n,n+1}$  encode the microscopic coupling between neighbouring chains. In the following, we consider two types of interchain coupling: parallel and skew.

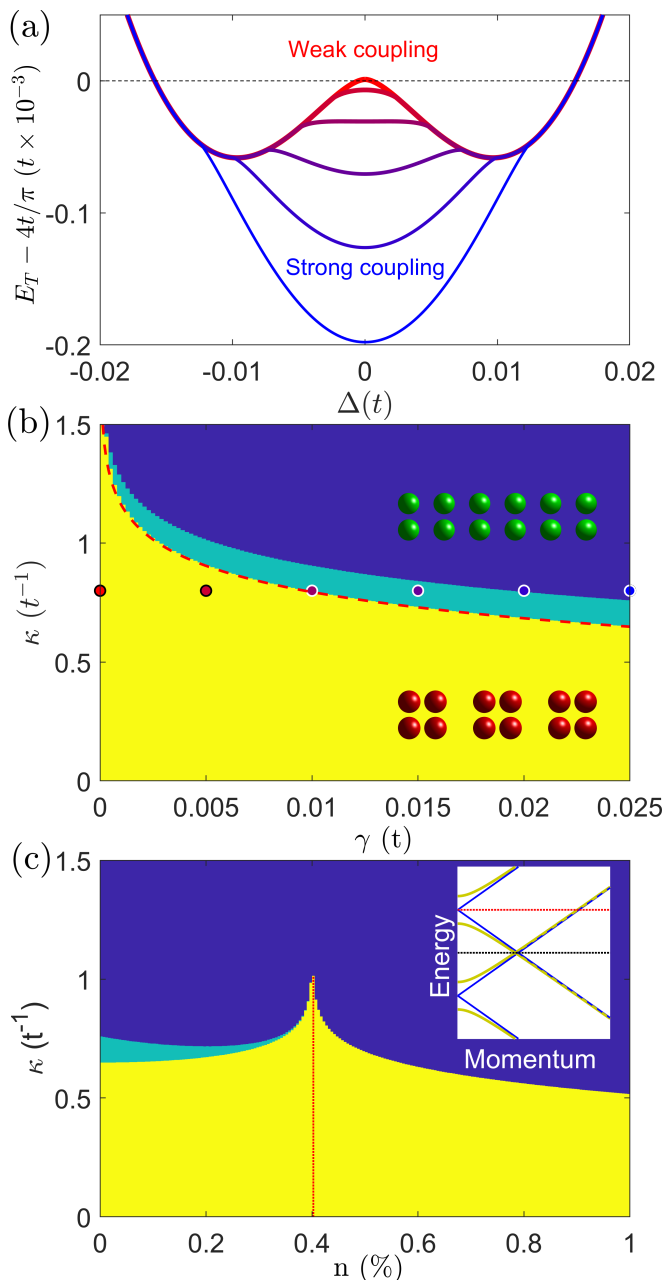


FIG. 2. (a) Total energy of two parallel-coupled atomic chains for different values of  $\gamma$ . As the coupling increases, the total energy transitions from two to three minima before  $\Delta = 0$  establishes as the global minimum. (b) Phase diagram of two parallel-coupled chains. In between the phase separation, there is a green region denoting bistability. (c) Phase diagram as a function of doping for  $\gamma = 0.025t$ . The level of doping at  $\sim 0.4\%$  that enhances the CDW order corresponds to the Fermi level at which a gap is opened in the band structure at the edge of the Brillouin zone  $k = -\pi/a$ , as shown in the inset.

### A. Parallel coupling

For parallel coupling, the chains are placed in an array such that each consecutive chain is a copy of the previous

chain translated perpendicularly to the chain direction by the same interchain distance. The interchain coupling matrix is  $T_{n,n+1} = \gamma \mathbb{I}_2$  in Eq. (7), where  $\gamma$  is the interchain hopping amplitude. Since the interchain hopping is proportional to the identity in sublattice space, the Hamiltonian can be written as

$$\mathcal{H} = \mathbb{I}_N \otimes H_k + H_\perp \otimes \mathbb{I}_2,$$

where  $H_\perp$  is the  $N \times N$  tridiagonal matrix describing the nearest neighbor hopping between chains. Diagonalizing  $H_\perp$  yields  $N$  decoupled Hamiltonians,

$$\mathcal{H} \rightarrow \mathbb{I}_N \otimes H_k + \text{diag}(\mu_1, \dots, \mu_n) \otimes \mathbb{I}_2, \quad (8)$$

$$\mu_n = 2\gamma \cos\left(\frac{n\pi}{N+1}\right), \quad n = 1, \dots, N.$$

Accordingly, the spectrum consists of rigidly shifted replicas of the single-chain dispersion,  $\beta|f_k| + \mu_n$ , that is, the parallel-coupled system is energetically equivalent to  $N$  independent 1D chains, each subject to an effective shift of the chemical potential,  $\mu_n$ .

The total energy of two parallel-coupled chains as a function of the dimerization amplitude  $\Delta$ , for different values of the coupling strength  $\gamma$ , is shown in Fig. 2(a). The corresponding band structure consists of two 1D atomic chain dispersions, shifted by  $\mu = \pm\gamma$ . For sufficiently strong interchain coupling, the undistorted configuration ( $\Delta = 0$ ) becomes the global minimum once the condition in Eq. (6) is met, while for weak interchain couplings the system features a double-well energy profile. For intermediate values of the interchain coupling, a local minimum at  $\Delta = 0$  emerges and coexists with another one at finite values of  $\Delta = \pm\Delta_0$ . In this situation, the system is bistable, and the complete phase diagram presented in Fig. 2(b), where we show the region of bistability in green, suggests that this behaviour is consistent across all values of the rigidity.

The stability of the CDW state under doping is also qualitatively modified compared to a single chain, where doping suppresses the Peierls distortion. Figure 2(c) shows the phase diagram as a function of the doping and rigidity. Initially, departure from half filling strengthens the CDW order up to a characteristic scale set by the interchain coupling,  $E_F = |\gamma|$ , where the Fermi level lies close to the band edge and the opening of a Peierls gap maximally lowers the electronic energy. At larger doping, the bistable regime disappears, and the system recovers the single-chain trend where doping weakens the CDW order.

Figure 3(a) generalizes the half filling phase diagram to stacks of  $N = 3, \dots, 6$  parallel-coupled chains. Bistability persists for all  $N$ . A key even-odd effect is also present: stacks with odd  $N$  never reach a fully metallic normal state. This follows from the transverse spectrum  $\mu_n$ , which for odd  $N$  must contain a mode with  $\mu_{(N+1)/2} = 0$ . One pair of effective single-chain bands, therefore, remains exactly at half filling, and retains a Peierls instability, even when the other modes are shifted away. This produces the weaker CDW phase with a marginal lattice distortion shown in light blue. By contrast, even- $N$  stacks exhibit phase diagrams closely analogous to the  $N = 2$  case (see appendix D for further discussion).

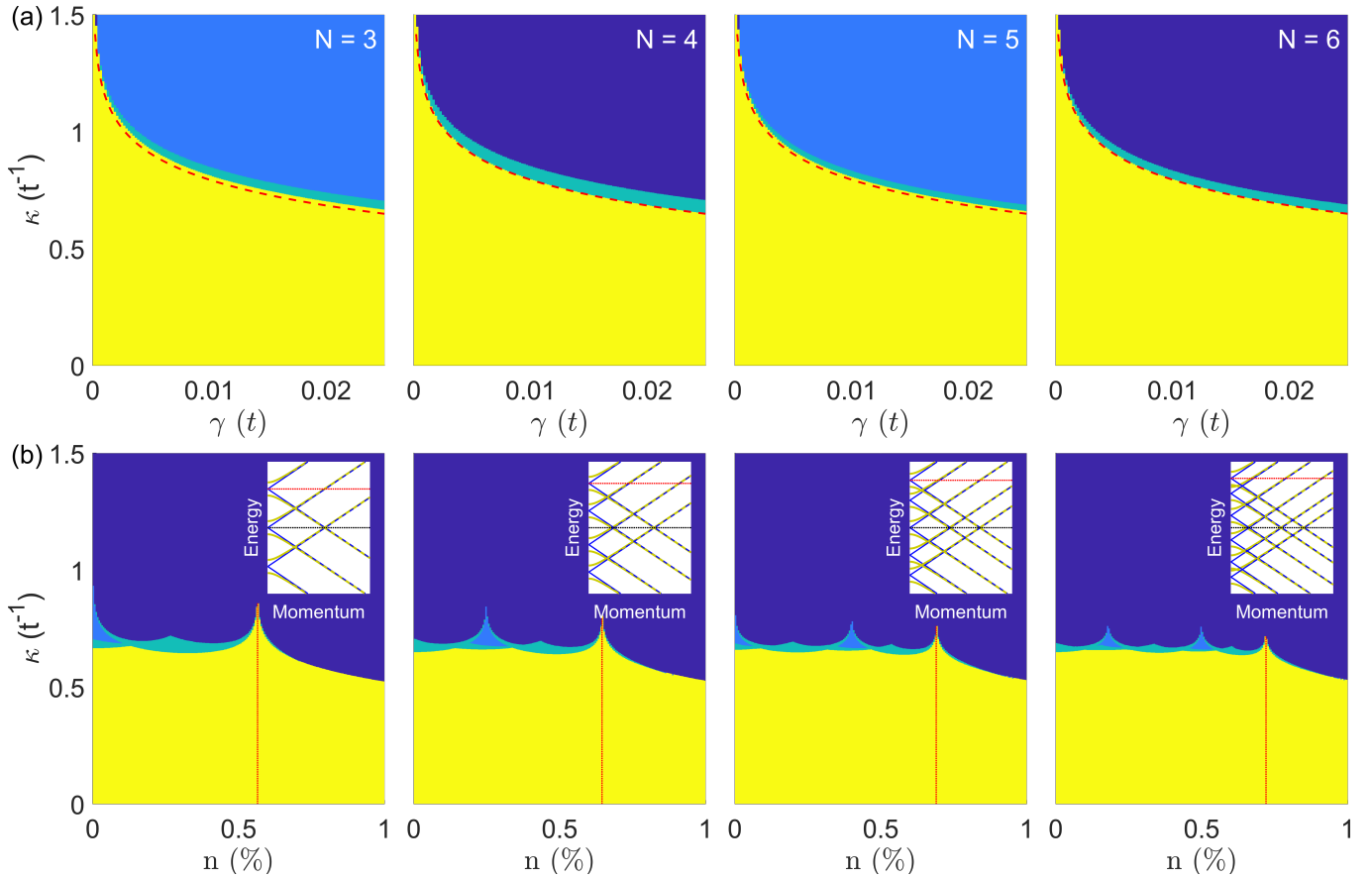


FIG. 3. (a) Phase diagram of parallel-coupled chains as a function interchain coupling  $\gamma$  and rigidity  $\kappa$ , with number of chains ranging from  $N = 3$  (leftmost) to  $N = 6$  (rightmost). Light blue represents a weak CDW order due to gapping of zero-energy bands that must exist for odd  $N$ , electron-hole symmetric spectra. All even-number chains share the same CDW/bistable regime phase boundary (see appendix D). (b) Phase diagram as a function of doping and rigidity, with  $\gamma = 0.025t$ . All subbands open a gap at the edge of the Brillouin zone  $k = -\pi/2a$ . The doping level at these energy points maximizes the energy reduction of the system and enhances the CDW order.

The corresponding doping-dependent phase diagrams for  $\gamma = 0.025t$  are shown in Fig. 3(b). Once the upper bands become significantly populated, all stacks display a monotonic suppression of CDW order with increasing doping. At lower doping, however, the phase boundaries develop a sequence of lobes that reflects the discrete set of transverse band edges. This behavior is consistent with the band structure shown in the insets: when the chemical potential lies close to a band degeneracy at the zone edge (red dotted line in the insets), the Peierls distortion is enhanced, leading to local strengthening of CDW order.

### B. Skew coupling

We now consider a skew-coupled geometry in which sites of chain  $n+1$  lie at the midpoints between consecutive sites of chain  $n$ . Each atom, therefore, hybridizes with its two nearest neighbors in the adjacent chain with equal amplitude  $\gamma$ . In contrast to parallel coupling, for  $N \geq 3$ , this geometry admits two distinct commensurate CDW stacking configurations, depending on the relative phase of the dimerization be-

tween neighboring chains. We refer to the configuration in which next-nearest chains are in phase as zig-zag (zzg) and to the configuration in which they are out of phase as nematic (nem).

In Eq. (7), the corresponding interchain hopping blocks take the form

$$T_{n,n+1}^{\text{zzg}} = \begin{cases} \gamma \begin{pmatrix} 1 & e^{2iak} \\ 1 & 1 \end{pmatrix}, & \text{for } n \text{ odd} \\ \gamma \begin{pmatrix} 1 & 1 \\ e^{-2iak} & 1 \end{pmatrix}, & \text{for } n \text{ even} \end{cases} \quad (9a)$$

$$T_{n,n+1}^{\text{nem}} = \gamma \begin{pmatrix} 1 & e^{2iak} \\ 1 & 1 \end{pmatrix}, \quad \forall n \quad (9b)$$

Unlike the parallel-coupled case, this Hamiltonian cannot be reduced to a direct sum of independent shifted single-atomic chains. We therefore determine the total energy and the equilibrium dimerization numerically.

Skew coupling qualitatively modifies the band structure by lifting the simple sublattice-exchange structure of the parallel-stacked geometry and producing additional band crossings near the Fermi level. While the spectrum of the undistorted

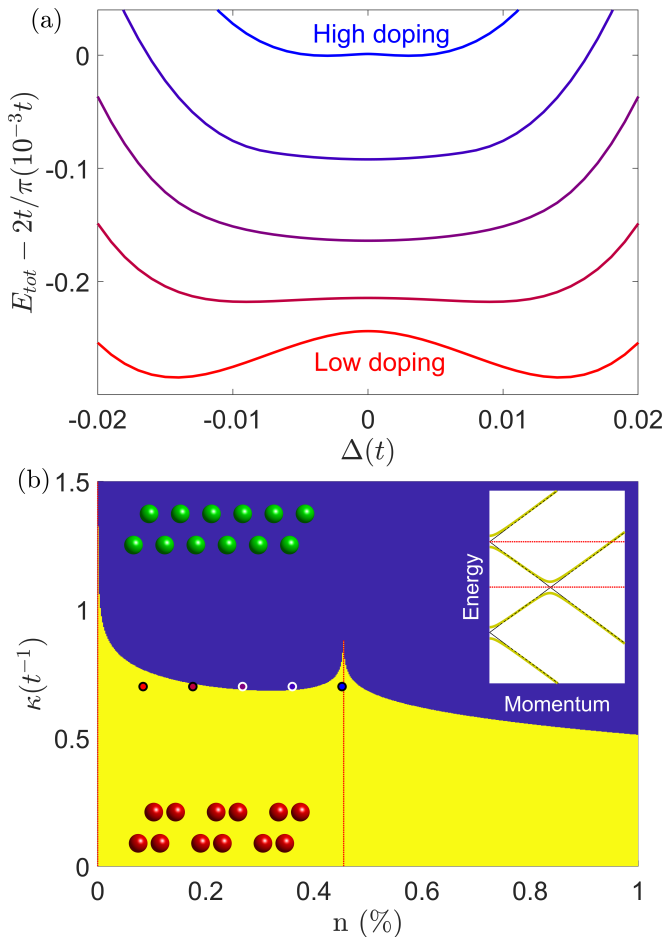


FIG. 4. (a) Total energy  $E_{tot}(\Delta)$  of two skew-coupled chains for  $\kappa = 0.7t^{-1}$  and  $\gamma = 0.02t$ , shown for several representative electron dopings. The evolution of the global minimum, from  $\Delta \neq 0$  to  $\Delta = 0$  and back to  $\Delta \neq 0$ , demonstrates reentrant CDW order. (b) Phase diagram as a function of electron doping  $n$  and rigidity  $\kappa$ . Inset: band structure near the Brillouin-zone edge, illustrating that CDW order is enhanced when the chemical potential lies close to a spectral gap (in particular at  $n = 0$  and  $n \simeq 0.45\%$ ).

phase remains gapless at these crossings, a finite dimerization  $\Delta \neq 0$  breaks sublattice symmetry and opens gaps at all of them. As a result, the competition between the elastic cost and the electronic energy gain from dimerization depends sensitively on the position of the chemical potential. Therefore, away from half filling, CDW order is not necessarily monotonic in doping. Instead, the CDW can be enhanced when the Fermi level approaches a band edge, and can even become reentrant if multiple gaps occur at different energies. This behaviour is illustrated in Fig. 4(a), which shows the total energy  $E(\Delta)$  for a skew-coupled double chain at several representative doping levels. At low doping (red curve), the energy is minimized at a finite distortion, while intermediate dopings suppress CDW. Upon further doping (blue line), the minimum reappears at  $\Delta \neq 0$ , demonstrating reentrant CDW order. The corresponding phase diagram is shown in Fig. 4(b). The reentrance occurs when the chemical potential

approaches a higher-energy spectral gap near the Brillouin-zone edge (inset), which restores the electronic energy gain from dimerization around  $n \simeq 0.45\%$ .

Finally, Fig. 5 shows the phase diagrams for skew-coupled stacks with  $N = 3, \dots, 6$  chains. In these systems the existence of two distinct CDW stackings produces a richer phase structure than in the parallel-coupled case. Nevertheless, the phase boundaries can be consistently interpreted in terms of the location and magnitude of band gaps in the electronic dispersion. At low doping, the zig-zag configuration is always preferred. At half filling, the relevant gap occurs at the Brillouin-zone edge and, in the zig-zag configuration, opens linearly with  $\Delta$ . In contrast, in the nematic configuration this gap is symmetry-suppressed at linear order and is generated only at second order, scaling as  $\Delta^2$  (see Appendix E). At moderate doping, however, the nematic stacking can open larger gaps at the relevant Fermi level, leading to an extended nematic-CDW region. At higher doping, the zig-zag phase reappears once the chemical potential approaches the next set of band edges. This sequence of transitions is consistent with the multiple avoided crossings visible in the band-structure insets of Fig. 5.

#### IV. CONCLUSIONS

In summary, we have studied the robustness of the Peierls instability under finite doping and interchain hybridization in finite-thickness arrays of identical atomic chains. We find that the interplay between doping, lattice rigidity, and transverse coupling produces a surprisingly rich phenomenology that goes well beyond the expectation of monotonic CDW suppression with doping. In parallel-coupled stacks, we identify a bistable regime where the normal and CDW-ordered configurations coexist as distinct local minima of the total energy. In skew-coupled geometries, multiple avoided crossings near the Fermi level lead to nonmonotonic doping dependence and signatures of reentrant CDW order.

This behavior is reminiscent of the complex CDW phase competition observed in quasi-two-dimensional materials, where multiple commensurate and incommensurate modulations may lie close in energy and evolve non-trivially with external control parameters [46–48]. More broadly, our results establish coupled atomic chains as a minimal platform that naturally bridges between the analytically transparent Peierls mechanism in one dimension and the richer energy landscapes typical of layered CDW compounds. In this sense, stacking geometry emerges as a simple microscopic control knob capable of generating metastability, bistability, and reentrant ordering even in the absence of additional strong-correlation ingredients.

#### ACKNOWLEDGMENTS

We acknowledge National Science and Technology Council (NSTC 112-2112-M-006-019-MY3) for financial support and

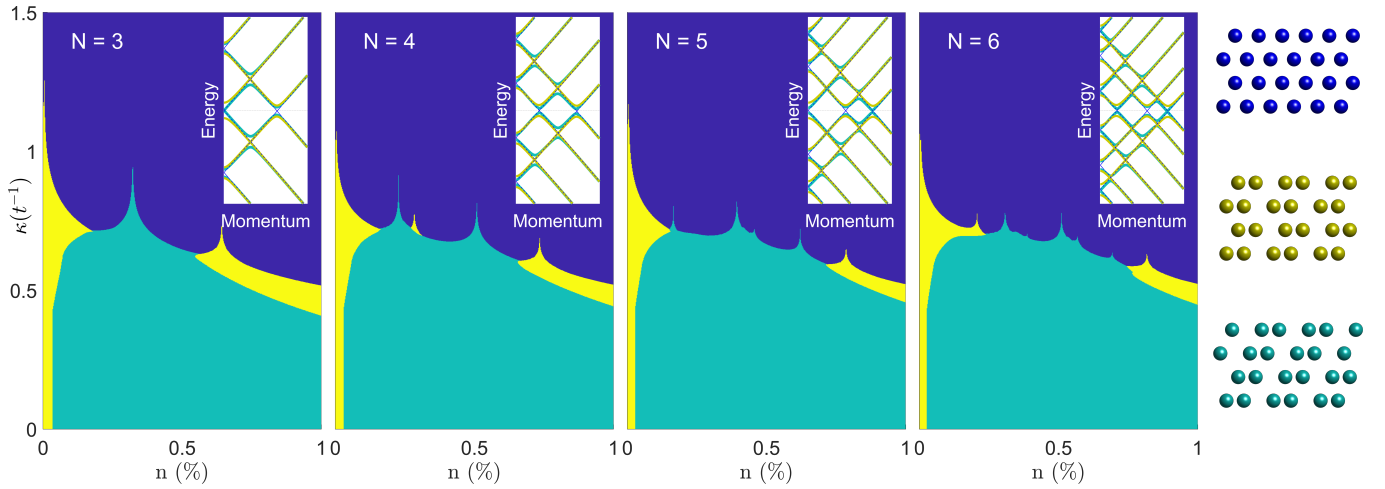


FIG. 5. Phase diagrams of skew-coupled stacks with  $N = 3, \dots, 6$  chains for  $\gamma = 0.02t$ , shown as a function of electron doping  $n$  and rigidity  $\kappa$ . The colors denote the ground state obtained from the global minimum of  $E_{\text{tot}}(\Delta)$ : normal state ( $\Delta = 0$ ), zig-zag CDW, and nematic CDW. Insets: corresponding band structures near the Brillouin-zone edge  $k = -\pi/2a$ . At low doping, the zig-zag configuration is favored, while at intermediate doping the nematic configuration becomes energetically preferred over an extended parameter range, consistent with the relative size and location of the spectral gaps.

National Center for High-performance Computing (NCHC) for providing computational and storage resources.

#### Appendix A: Connection to mean-field theory

Here, we demonstrate that the Hamiltonian employed in Eq. (1) is equivalent to that derived from the mean-field theory. The general form of the Hamiltonian of a one-dimensional chain of single-orbital atoms with inter-atomic spacing  $a$ , occupied by spinless electrons, in the framework of second quantization reads

$$\begin{aligned}
 H_{1D} &= H_{\text{el}} + H_{\text{ph}} + H_{\text{el-ph}} & (\text{A1}) \\
 H_{\text{el}} &= \sum_k \epsilon_k \hat{c}_k^\dagger \hat{c}_k \\
 H_{\text{ph}} &= \sum_q \hbar\omega_q \hat{b}_{-q}^\dagger \hat{b}_q \\
 H_{\text{el-ph}} &= \sum_{\langle k,q \rangle} g(k,q) \hat{c}_{k+q}^\dagger \hat{c}_k \left( \hat{b}_{-q}^\dagger + \hat{b}_q \right),
 \end{aligned}$$

where  $\hat{c}_k^\dagger$  ( $\hat{c}_k$ ) and  $\hat{b}_q^\dagger$  ( $\hat{b}_q$ ) are the operators that create (destroy) an electron and a phonon with momentum  $k$  and  $q$ , respectively. Above, we also introduce the electronic dispersion  $\epsilon_k = 2t \cos(ka)$  of the electron gas, with  $t$  being the hopping constant. At half filling, the Fermi surface is nested by the vector  $2k_F = \pi/a$ , and at zero temperature, the Peierls instability is associated with condensation of the phonon mode at  $q = \pm 2k_F$ . To reduce the Hamiltonian above into a bilinear form, we assume the electron-phonon coupling  $g(k,q) = g$  is constant, and define the order parameter  $\eta = g/\sqrt{L} \langle \hat{b}_{2k_F} + \hat{b}_{-2k_F}^\dagger \rangle$ . After mean-field decoupling and diagonalization in the reduced Brillouin zone, the mean-field couples electronic states at  $k$  and  $k + \pi/2a$ , yielding the effective two-component basis of right/left movers,  $(\hat{c}_{+,k}^\dagger; \hat{c}_{-,k}^\dagger)$ .

The resulting Hamiltonian takes the form[49]

$$\mathcal{H}_{1D}^{\text{MF}} = \begin{pmatrix} \epsilon_k^+ & \eta \\ \eta & \epsilon_k^- \end{pmatrix} = \sigma \cdot \mathbf{d}_{\text{MF}}, \quad (\text{A2})$$

$$\begin{aligned} \mathbf{d}_{\text{MF}} &= (\eta, 0, \epsilon_k) = \sqrt{\epsilon_k^2 + \eta^2} [\sin(\varphi_k), 0, \cos(\varphi_k)], \\ \sin(\varphi_k) &= \frac{\eta}{\sqrt{\epsilon_k^2 + \eta^2}}, \quad \cos(\varphi_k) = \frac{\epsilon_k}{\sqrt{\epsilon_k^2 + \eta^2}} \end{aligned} \quad (\text{A3})$$

Above, we chose a gauge where the order parameter is real. In the same language, we can re-express the Hamiltonian in Eq. (1) as

$$\begin{aligned} \mathcal{H}_{\text{SSH}} &= \sigma \cdot \mathbf{d}_{\text{SSH}} \quad (\text{A4}) \\ \mathbf{d}_{\text{SSH}} &= [\text{Re}(f_k), -\text{Im}(f_k), 0], \\ &= |f_k| [\cos(\theta_k), -\sin(\theta_k), 0], \end{aligned}$$

where  $f_k = \sqrt{\epsilon_k^2 + \delta^2 \sin^2(ka)} e^{i\theta_k} \approx \sqrt{\epsilon_k^2 + \delta^2} e^{i\theta_k}$  in the vicinity of the Brillouin zone edge. Both  $H_{\text{MF}}$  and  $H_{\text{SSH}}$  are traceless, and the 3D vectors  $\mathbf{d}_{\text{MF}}$  and  $\mathbf{d}_{\text{SSH}}$  have the same length, thus there must exist a rotation  $R(k) \in SO(3)$ , such that  $\mathcal{U}(\sigma \cdot \mathbf{d}_{\text{SSH}})\mathcal{U}^\dagger = \sigma \cdot \mathbf{d}_{\text{MF}}$ . To note, this unitary transformation is allowed to be  $k$ -dependent, reflecting the freedom to choose a  $k$ -dependent Bloch basis in the two-component sublattice space. We can construct this unitary transformation by composing two rotations: the first one being a rotation in the  $xy$ -plane that removes the  $y$ -component,

$$\begin{aligned} \mathcal{U}_1 H_{\text{SSH}} \mathcal{U}_1^\dagger &= |f_k| \sigma_x, \quad (\text{A5}) \\ \mathcal{U}_1(k) &= \exp(i \frac{\theta_k}{2} \sigma_z), \end{aligned}$$

and the second one being a rotation of the Hamiltonian by an angle  $\varphi_k$ ,

$$\begin{aligned} \mathcal{U}_2 |f_k| \sigma_x \mathcal{U}_2^\dagger &= |f_k| [\sin \varphi_k \sigma_x + \cos \varphi_k \sigma_z] \equiv H_{\text{MF}}, \quad (\text{A6}) \\ \mathcal{U}_2 &= \exp(-i \frac{\varphi_k}{2} \sigma_y). \end{aligned}$$

Therefore, the unitary matrix  $\mathcal{U}(k) = \mathcal{U}_2(k)\mathcal{U}_1(k)$  transforms the SSH Hamiltonian in Eq. (1), written in the basis of A/B dimer sublattices, into the Hamiltonian in Eq. (A2), written in the basis of right/left movers. The two Hamiltonians are unitarily equivalent after identifying the MF order parameter  $\eta$  with the low-energy dimerization gap  $\delta$ .

### Appendix B: Analytical minimum of the total energy

At half filling, the total energy per unit cell ( $2a$ ) is given by the sum of elastic and band contributions,

$$\frac{E_{\text{tot}}}{N} = \frac{K\delta^2}{\alpha^2} - \frac{1}{N} \sum_{k=-\frac{\pi}{2a}}^{\frac{\pi}{2a}} \sqrt{t_+^2 + t_-^2 + 2t_+t_- \cos(2ka)}, \quad (\text{B1})$$

In the thermodynamic limit,  $\frac{1}{N} \sum_k \rightarrow \frac{2a}{2\pi} \int dk$ , and the band contribution becomes

$$\begin{aligned} \frac{E_{\text{band}}}{N} &= -\frac{a}{\pi} \int_{-\frac{\pi}{2a}}^{\frac{\pi}{2a}} dk \sqrt{t_+^2 + t_-^2 + 2t_+t_- \cos(2ka)} \quad (\text{B2}) \\ &= -\frac{1}{\pi} \int_{-\pi/2}^{\pi/2} d\phi \sqrt{4t^2 \cos^2 \phi + \delta^2 \sin^2 \phi}, \quad (\text{B3}) \end{aligned}$$

where we define  $\phi = ka$ . Introducing the dimensionless dimerization parameter  $\Delta \equiv \delta/2t$ , we obtain

$$\frac{E_{\text{band}}}{N} = -\frac{2t}{\pi} \int_{-\frac{\pi}{2}}^{\frac{\pi}{2}} d\phi \sqrt{1 - (1 - \Delta^2) \sin^2 \phi} \quad (\text{B4})$$

$$= -\frac{4t}{\pi} \mathcal{E}(\sqrt{1 - \Delta^2}), \quad (\text{B5})$$

where  $\mathcal{E}(k)$  denotes the complete elliptic integral of the second kind. It is convenient to write the total energy in the dimensionless form

$$\frac{E_{\text{tot}}}{N} = 4t^2 \kappa \Delta^2 - \frac{4t}{\pi} \mathcal{E}(\sqrt{1 - \Delta^2}), \quad (\text{B6})$$

where  $\kappa \equiv \frac{K}{4t^2 \alpha^2}$ . For  $\Delta \ll 1$ , that is, close to the uniform chain, the elliptic integral admits the standard expansion

$$\mathcal{E}(\sqrt{1 - \Delta^2}) = 1 + \frac{\Delta^2}{2} \left[ \ln\left(\frac{4}{\Delta}\right) - \frac{1}{2} \right] + O(\Delta^4 \ln \Delta). \quad (\text{B7})$$

Substituting Eq. (B7) into Eq. (B6) yields

$$\frac{E_{\text{tot}}}{N} \simeq 4t^2 \kappa \Delta^2 - \frac{4t}{\pi} \left\{ 1 + \frac{\Delta^2}{2} \left[ \ln\left(\frac{4}{\Delta}\right) - \frac{1}{2} \right] \right\}. \quad (\text{B8})$$

The stationary points satisfy  $\partial_\Delta (E_{\text{tot}}/N) = 0$ ,

$$8t^2 \kappa \Delta - \frac{4t}{\pi} \Delta \left[ \ln\left(\frac{4}{\Delta}\right) - 1 \right] = 0. \quad (\text{B9})$$

Besides the trivial solution  $\Delta = 0$ , this equation admits a nonzero solution,

$$\Delta_0 = \frac{4}{e} e^{-2\pi t \kappa}. \quad (\text{B10})$$

### Appendix C: Expansion of the incomplete elliptic integral

Here we derive the analytical expression for the incomplete elliptic integral appearing in Eq. (5). We consider

$$\tilde{\mathcal{E}}(\epsilon, \Delta) \equiv \int_0^{\frac{\pi}{2} - \epsilon} d\phi \sqrt{1 - (1 - \Delta^2) \sin^2 \phi}, \quad (\text{C1})$$

which can be written as a complete elliptic integral of the second kind minus a tail contribution,

$$\tilde{\mathcal{E}}(\epsilon, \Delta) = \mathcal{E}(\sqrt{1 - \Delta^2}) - I(\epsilon, \Delta), \quad (\text{C2})$$

where  $\mathcal{E}(k) \equiv \int_0^{\pi/2} d\phi \sqrt{1 - k^2 \sin^2 \phi}$  and

$$I(\epsilon, \Delta) \equiv \int_{\frac{\pi}{2} - \epsilon}^{\frac{\pi}{2}} d\phi \sqrt{1 - (1 - \Delta^2) \sin^2 \phi}. \quad (\text{C3})$$

Introducing  $\phi \rightarrow \frac{\pi}{2} - \phi$  in the tail integral yields

$$I(\epsilon, \Delta) = \int_0^\epsilon d\phi \sqrt{1 - (1 - \Delta^2) \cos^2 \phi}. \quad (\text{C4})$$

For  $\epsilon \ll 1$ , the integrand can be expanded to leading order as  $[1 - (1 - \Delta^2) \cos^2 \phi]^{1/2} \approx [\Delta^2 + (1 - \Delta^2) \phi^2]^{1/2}$ . This approximation amounts to dropping the term  $-(1 - \Delta^2) \phi^4/3$ . Requiring such term to remain small compared to  $\Delta^2$  over  $\phi \in [0, \epsilon]$  implies the additional condition  $\epsilon \ll \Delta^{1/2}$ . With this truncation, the integral reads

$$\begin{aligned} I(\epsilon, \Delta) &\simeq \int_0^\epsilon d\phi \sqrt{\Delta^2 + (1 - \Delta^2) \phi^2} \\ &= \sqrt{1 - \Delta^2} \int_0^\epsilon d\phi \sqrt{\phi^2 + C^2}, \end{aligned} \quad (\text{C5})$$

where we defined  $C^2 \equiv \frac{\Delta^2}{1 - \Delta^2}$ . The remaining integral can be evaluated analytically using hyperbolic trigonometric functions,

$$\begin{aligned} I(\epsilon, \Delta) &\approx \frac{\sqrt{1 - \Delta^2}}{2} \left[ \epsilon \sqrt{\epsilon^2 + C^2} + C^2 \ln \left( \frac{\epsilon + \sqrt{\epsilon^2 + C^2}}{C} \right) \right] \\ &\approx \frac{1}{2} \left[ \epsilon \sqrt{\epsilon^2 + \Delta^2} + \Delta^2 \ln \left( \frac{\epsilon + \sqrt{\epsilon^2 + \Delta^2}}{\Delta} \right) \right]. \end{aligned} \quad (\text{C6})$$

where only in the last step  $\Delta \ll 1$  was assumed. Keeping only the leading term in the endpoint expansion provides a uniform approximation that captures the logarithmic dependence on  $\Delta$  as  $\Delta \rightarrow 0$ . The expression above coincides with the regularizing term appearing in Eq. (5).

#### Appendix D: Phase diagram of 2N parallel-coupled chains

In the main text, we pointed out that all systems consisting of  $2N$  parallel-coupled chains share the same phase diagram. Here we rationalize this empirical observation by explicitly computing the critical inter-chain coupling  $\gamma_c$  above which the charge-density-wave (CDW) state becomes unstable. To this end, we evaluate the total-energy difference between the CDW and the normal state,

$$\delta E_{\text{T}}^{2N}(\Delta) \equiv E_{\text{T}}^{2N}(\Delta) - E_{\text{T}}^{2N}(0). \quad (\text{D1})$$

For  $\Delta = 0$  the total energy reads

$$E_{\text{T}}^{2N}(0) = -\frac{8t}{\pi} N + \frac{4t}{\pi} \sum_{n=1}^N \epsilon_n^2, \quad (\text{D2})$$

where  $\epsilon_n$  accounts for the band-edge shift induced by the inter-chain hybridization. For finite  $\Delta$  we obtain

$$E_{\text{T}}^{2N}(\Delta) = 8Nt^2 \kappa \Delta^2 - \frac{8t}{\pi} \sum_{n=1}^N \int_0^{\pi/2 - \epsilon_n} d\phi \sqrt{1 - (1 - \Delta^2) \sin^2 \phi}. \quad (\text{D3})$$

Expanding the elliptic integral for  $\Delta \ll 1$ , this expression can be written as

$$E_{\text{T}}^{2N}(\Delta) = 8Nt^2 \kappa \Delta^2 - \frac{8t}{\pi} N \left[ 1 + \frac{\Delta^2}{2} \left( \ln \frac{4}{\Delta} - \frac{1}{2} \right) \right] + \frac{4t}{\pi} \sum_{n=1}^N \left[ \epsilon_n \sqrt{\epsilon_n^2 + \Delta^2} + \Delta^2 \ln \left( \frac{\epsilon_n + \sqrt{\epsilon_n^2 + \Delta^2}}{\Delta} \right) \right]. \quad (\text{D4})$$

For odd  $N$  parallel-coupled chains at half filling, one pair of bands has  $\epsilon = 0$ , and the logarithmic singularity survives, driving a Peierls-like instability (see light blue region in Fig. 3). For an even number of coupled chains, however, the transverse dispersion shift

$$\epsilon_n = 2\gamma \cos \left( \frac{n\pi}{2N + 1} \right), \quad (\text{D5})$$

is never zero for integer  $n \in [1, N]$ , and the divergence is therefore regularized. Since the CDW gap is the smallest en-

ergy scale in our problem ( $\Delta \sim 10^{-6}t$ ), we expand the total energy to leading order in  $\Delta$ . After straightforward algebra we obtain

$$\delta E_{\text{T}}^{2N}(\Delta) = \frac{4t\Delta^2}{\pi} \left[ 2Nt\kappa\pi + N(1 - \ln 2) + \sum_{n=1}^N \ln \left( \frac{\epsilon_n}{t} \right) \right]. \quad (\text{D6})$$

Using  $\epsilon_n \simeq (\gamma/t) \cos \left( \frac{n\pi}{2N+1} \right)$ , the transition line is obtained by imposing  $\delta E_{\text{T}}^{2N}(\Delta) = 0$ , which yields

$$2t\kappa\pi + (1 - \ln 2) + \ln\left(\frac{\gamma}{t}\right) + \frac{1}{N} \sum_{n=1}^N \ln \left[ \cos\left(\frac{n\pi}{2N+1}\right) \right] = 0. \quad (\text{D7})$$

At first sight, Eq. (D7) appears to depend on  $N$  through the last term. However, this dependence cancels exactly. To show this, we write the polynomial  $z^{2N+1} + 1$  as a product over its roots,

$$z^{2N+1} + 1 = \prod_{j=0}^{2N} (z - e^{i\theta_j}), \quad \theta_j = \frac{(2j+1)\pi}{2N+1}. \quad (\text{D8})$$

Evaluating at  $z = 1$  gives

$$2 = \prod_{j=0}^{2N} (1 - e^{i\theta_j}). \quad (\text{D9})$$

The factor with  $j = N$  corresponds to  $\theta_N = \pi$  and thus equals  $1 - e^{i\pi} = 2$ . Factoring it out, we obtain

$$1 = \prod_{j \neq N} (1 - e^{i\theta_j}). \quad (\text{D10})$$

Using  $\theta_{2N-j} = 2\pi - \theta_j$ , we can pair complex conjugates and write

$$1 = \prod_{j=0}^{N-1} (1 - e^{i\theta_j})(1 - e^{-i\theta_j}) = \prod_{j=0}^{N-1} 4 \sin^2\left(\frac{\theta_j}{2}\right). \quad (\text{D11})$$

Taking the square root yields

$$\prod_{j=0}^{N-1} \sin\left(\frac{\theta_j}{2}\right) = 2^{-N}. \quad (\text{D12})$$

Finally, since

$$\sin\left(\frac{\theta_j}{2}\right) = \sin\left[\frac{(2j+1)\pi}{2(2N+1)}\right] = \cos\left[\frac{(j+1)\pi}{2N+1}\right], \quad (\text{D13})$$

we obtain the identity

$$\prod_{n=1}^N \cos\left(\frac{n\pi}{2N+1}\right) = 2^{-N}. \quad (\text{D14})$$

Therefore,

$$\frac{1}{N} \sum_{n=1}^N \ln \left[ \cos\left(\frac{n\pi}{2N+1}\right) \right] = \frac{1}{N} \ln(2^{-N}) = -\ln 2, \quad (\text{D15})$$

which is independent of  $N$ . This proves that the critical coupling  $\gamma_c$  obtained from Eq. (D7) is the same for all  $2N$ -chain systems, consistent with the  $N$ -independent phase diagram reported in the main text.

## Appendix E: Zig-zag and nematic phases at half-filling

In this appendix we provide a simple perturbative argument showing that, at half filling, the zig-zag configuration is energetically favored over the nematic one. We focus on the minimal case of  $N = 3$  skew-coupled chains and evaluate the Hamiltonian at the Brillouin-zone corner  $k = -\pi/2a$ , where the Peierls distortion is expected to open a gap.

At  $k = -\pi/2a$ , the nematic and zig-zag Hamiltonians read

$$H_{k=-\frac{\pi}{2a}}^{\text{nem}} = \begin{pmatrix} \delta\sigma_x & T & 0 \\ T^\dagger & \delta\sigma_x & T \\ 0 & T^\dagger & \delta\sigma_x \end{pmatrix}, \quad (\text{E1a})$$

$$H_{k=-\frac{\pi}{2a}}^{\text{zzg}} = \begin{pmatrix} \delta\sigma_x & T & 0 \\ T^\dagger & \delta\sigma_x & T^\dagger \\ 0 & T & \delta\sigma_x \end{pmatrix}, \quad (\text{E1b})$$

where the inter-chain coupling is

$$T = \gamma \begin{pmatrix} 1 & -1 \\ 1 & 1 \end{pmatrix} = \gamma(\sigma_x - i\sigma_y). \quad (\text{E2})$$

We consider the Peierls term as a small perturbation,

$$V = \delta \text{diag}(\sigma_x, \sigma_x, \sigma_x), \quad (\text{E3})$$

and define the unperturbed Hamiltonians ( $\delta = 0$ ),

$$H^{\text{nem}(0)} = \begin{pmatrix} 0 & T & 0 \\ T^\dagger & 0 & T \\ 0 & T^\dagger & 0 \end{pmatrix}, \quad (\text{E4a})$$

$$H^{\text{zzg}(0)} = \begin{pmatrix} 0 & T & 0 \\ T^\dagger & 0 & T^\dagger \\ 0 & T & 0 \end{pmatrix}. \quad (\text{E4b})$$

Both  $H_{\text{nem}}^{(0)}$  and  $H_{\text{zzg}}^{(0)}$  host a twofold degenerate eigenvalue at  $E^{(0)} = 0$ . The corresponding eigenstates can be constructed explicitly by taking a spinor  $\phi$  on the first chain and requiring the middle-chain component to vanish. Then the zero-energy eigenvectors read,

$$\Psi_{\text{nem}} = \frac{1}{\sqrt{2}} \begin{pmatrix} \phi \\ 0 \\ -i\sigma_y\phi \end{pmatrix}, \quad \Psi_{\text{zzg}} = \frac{1}{\sqrt{2}} \begin{pmatrix} \phi \\ 0 \\ -\phi \end{pmatrix},$$

Since the zero-energy eigenspace is two-dimensional, the first-order spectrum is obtained by diagonalizing the perturbation restricted to this subspace [50]. For the *nematic configuration*, the matrix elements of the first-order perturbation in

the degenerate subspace are

$$V_{\text{eff}}^{(\text{nem})} = \langle \Psi_{\text{nem}} | V | \Psi_{\text{nem}} \rangle \quad (\text{E6})$$

$$= \frac{\delta}{2} [\sigma_x + (-i\sigma_y)^\dagger \sigma_x (-i\sigma_y)] = 0. \quad (\text{E7})$$

Therefore the degeneracy at  $E^{(0)} = 0$  is not lifted at first order in  $\delta$  in the nematic configuration,  $E_{\text{nem}}^{(1)} = 0$ . For the *zig-zag configuration*, however, the effective perturbation becomes

$$V_{\text{eff}}^{(\text{nem})} = \langle \Psi_{\text{nem}} | V | \Psi_{\text{nem}} \rangle \quad (\text{E8})$$

$$= \frac{\delta}{2} [\sigma_x + \sigma_x] = \delta\sigma_x. \quad (\text{E9})$$

Diagonalizing the matrix above yields the first-order energies  $E_{\text{zzg}}^{(1)} = \pm\delta$ . Hence, in the zig-zag configuration the twofold degeneracy is lifted already at first order, producing a linear-in- $\delta$  splitting at the Brillouin-zone corner. A larger splitting produces a larger lowering of the occupied energies, which always translates into a stronger Peierls CDW phase. Since the nematic configuration shows no first-order splitting, while the zig-zag configuration splits as  $2\delta$  at  $k = -\pi/2a$ , we conclude that the zig-zag phase is energetically preferred at (and near) half filling.

- 
- [1] Y. Cao, V. Fatemi, S. Fang, K. Watanabe, T. Taniguchi, E. Kaxiras, and P. Jarillo-Herrero, *Nature* **556**, 43 (2018).
- [2] L. Wang, E.-M. Shih, A. Ghiotto, L. Xian, D. A. Rhodes, C. Tan, M. Claassen, D. M. Kennes, Y. Bai, B. Kim, K. Watanabe, T. Taniguchi, X. Zhu, J. Hone, A. Rubio, A. N. Pasupathy, and C. R. Dean, *Nature Materials* **19**, 861 (2020).
- [3] P. A. Pantaleon, A. Jimeno-Pozo, H. Sainz-Cruz, V. T. Phong, T. Cea, and F. Guinea, *Nature Reviews Physics* **5**, 304 (2023).
- [4] R. Su, M. Kuiri, K. Watanabe, T. Taniguchi, and J. Folk, *Nature Materials* **22**, 1332 (2023).
- [5] S. Xu, M. M. Al Ezzi, N. Balakrishnan, A. Garcia-Ruiz, B. Tsim, C. Mullan, J. Barrier, N. Xin, B. A. Piot, T. Taniguchi, K. Watanabe, A. Carvalho, A. Mishchenko, A. K. Geim, V. I. Falko, S. Adam, A. H. C. Neto, K. S. Novoselov, and Y. Shi, *Nature Physics* **17**, 619 (2021).
- [6] S. Paschen and Q. Si, *Nature Reviews Physics* **3**, 9 (2021).
- [7] Y. Yanase, T. Jujo, T. Nomura, H. Ikeda, T. Hotta, and K. Yamada, *Physics Reports* **387**, 1 (2003).
- [8] W. A. Little, *Physical Review* **134**, A1416 (1964).
- [9] P. W. Anderson, *Physical Review* **109**, 1492 (1958).
- [10] J. Li, R.-L. Chu, J. K. Jain, and S.-Q. Shen, *Physical Review Letters* **102**, 136806 (2009).
- [11] C. W. Groth, M. Wimmer, A. R. Akhmerov, J. Tworzydło, and C. W. J. Beenakker, *Physical Review Letters* **103**, 196805 (2009).
- [12] C. P. Orth, T. Sekera, C. Bruder, and T. L. Schmidt, *Scientific Reports* **6**, 24007 (2016).
- [13] Y.-B. Yang, K. Li, L.-M. Duan, and Y. Xu, *Physical Review B* **103**, 085408 (2021).
- [14] S.-N. Liu, G.-Q. Zhang, L.-Z. Tang, and D.-W. Zhang, *Physics Letters A* **431**, 128004 (2022).
- [15] W. Kohn, *Physical Review Letters* **2**, 393 (1959).
- [16] S. Piscanec, M. Lazzeri, F. Mauri, A. C. Ferrari, and J. Robertson, *Physical Review Letters* **93**, 185503 (2004).
- [17] M. Hoesch, A. Bosak, D. Chernyshov, H. Berger, and M. Krisch, *Physical Review Letters* **102**, 086402 (2009).
- [18] H. Ochoa, *Physical Review B* **100**, 155426 (2019).
- [19] J. Birkbeck, J. Xiao, A. Inbar, T. Taniguchi, K. Watanabe, E. Berg, L. Glazman, F. Guinea, F. von Oppen, and S. Ilani, *Nature* **641**, 345 (2025).
- [20] G. Gruner, *Reviews of Modern Physics* **60**, 1129 (1988).
- [21] M. D. Johannes and I. I. Mazin, *Physical Review B* **77**, 165135 (2008).
- [22] X. Zhu, Y. Cao, J. Zhang, E. W. Plummer, and J. Guo, *Proceedings of the National Academy of Sciences* **112**, 2367 (2015).
- [23] Y.-T. Huang, Z.-Z. Li, N.-K. Chen, Y. Wang, H.-B. Sun, S. Zhang, and X.-B. Li, *Nature Communications* **15**, 9983 (2024).
- [24] Y. Chen, W. Ruan, M. Wu, S. Tang, H. Ryu, H.-Z. Tsai, R. L. Lee, S. Kahn, F. Liou, C. Jia, O. R. Albertini, H. Xiong, T. Jia, Z. Liu, J. A. Sobota, A. Y. Liu, J. E. Moore, Z.-X. Shen, S. G. Louie, S.-K. Mo, and M. F. Crommie, *Nature Physics* **16**, 218 (2020).
- [25] H. Ryu, Y. Chen, H. Kim, H.-Z. Tsai, S. Tang, J. Jiang, F. Liou, S. Kahn, C. Jia, A. A. Omrani, J. H. Shim, Z. Hussain, Z.-X. Shen, K. Kim, B. I. Min, C. Hwang, M. F. Crommie, and S.-K. Mo, *Nano Letters* **18**, 689 (2018).
- [26] W. R. B. Luckin, Y. Li, J. Jiang, S. M. Gunasekera, C. Wen, Y. Zhang, D. Prabhakaran, F. Flicker, Y. Chen, and M. Mucha-Kruczynski, *Physical Review Research* **6**, 013088 (2024).
- [27] Y. Nakata, K. Sugawara, A. Chainani, H. Oka, C. Bao, S. Zhou, P.-Y. Chuang, C.-M. Cheng, T. Kawakami, Y. Saruta, T. Fukumura, S. Zhou, T. Takahashi, and T. Sato, *Nature Communications* **12**, 5873 (2021).
- [28] D. Lin, S. Li, J. Wen, H. Berger, L. Forro, H. Zhou, S. Jia, T. Taniguchi, K. Watanabe, X. Xi, and M. S. Bahramy, *Nature Communications* **11**, 2406 (2020).
- [29] F. H. Yu, D. H. Ma, W. Z. Zhuo, S. Q. Liu, X. K. Wen, B. Lei, J. J. Ying, and X. H. Chen, *Nature Communications* **12**, 3645 (2021).
- [30] Y. Qi, Q. Yang, P. Zhu, D. Hu, X. Chen, H. Ren, P. Duan, J. Xiao, Z. Wang, and X. Li, *Journal of Materials Chemistry C* (2026), 10.1039/D5TC03422A.
- [31] Y. Hu, X. Wu, B. R. Ortiz, X. Han, N. C. Plumb, S. D. Wilson, A. P. Schnyder, and M. Shi, *Physical Review B* **106**, L241106 (2022).
- [32] J. Luo, Z. Zhao, Y. Z. Zhou, J. Yang, A. F. Fang, H. T. Yang, H. J. Gao, R. Zhou, and G.-q. Zheng, *npj Quantum Materials* **7**, 30 (2022).
- [33] G. Gye, E. Oh, and H. W. Yeom, *Physical Review Letters* **122**, 016403 (2019).
- [34] B. Guster, C. Rubio-Verdu, R. Robles, J. Zaldivar, P. Dreher, M. Pruneda, J. A. Silva-Guillen, D.-J. Choi, J. I. Pascual, M. M. Ugeda, P. Ordejon, and E. Canadell, *Nano Letters* **19**, 3027 (2019).
- [35] T.-R. T. Han, F. Zhou, C. D. Malliakas, P. M. Duxbury, S. D. Mahanti, M. G. Kanatzidis, and C.-Y. Ruan, *Science Advances* **1**, e1400173 (2015).

- [36] L. Stojchevska, P. Sutar, E. Goreshnik, D. Mihailovic, and T. Mertelj, *Physical Review B* **98**, 195121 (2018).
- [37] M. Huber, S. Zuber, V. Rosa-Rocha, S. C. Haley, N. Dale, L. Moreschini, D.-H. Lee, A. Bostwick, C. Jozwiak, J. G. Analytis, and A. Lanzara, *Communications Physics* **8**, 469 (2025).
- [38] B. Q. Lv, A. Zong, D. Wu, A. V. Rozhkov, B. V. Fine, S.-D. Chen, M. Hashimoto, D.-H. Lu, M. Li, Y.-B. Huang, J. P. C. Ruff, D. A. Walko, Z. H. Chen, I. Hwang, Y. Su, X. Shen, X. Wang, F. Han, H. C. Po, Y. Wang, P. Jarillo-Herrero, X. Wang, H. Zhou, C.-J. Sun, H. Wen, Z.-X. Shen, N. L. Wang, and N. Gedik, *Physical Review Letters* **128**, 036401 (2022).
- [39] A. K. Geremew, S. Rumyantsev, B. Debnath, R. K. Lake, and A. A. Balandin, *Applied Physics Letters* **116**, 163101 (2020).
- [40] D. Mihailovic, D. Svetin, I. Vaskivskiy, R. Venturini, B. Lipovsek, and A. Mraz, *Applied Physics Letters* **119**, 013106 (2021).
- [41] T. Patel, J. Okamoto, T. Dekker, B. Yang, J. Gao, X. Luo, W. Lu, Y. Sun, and A. W. Tsen, *Nano Letters* **20**, 7200 (2020).
- [42] R. E. Peierls, *Quantum Theory of Solids* (Clarendon Press, 1955).
- [43] W. P. Su, J. R. Schrieffer, and A. J. Heeger, *Physical Review Letters* **42**, 1698 (1979).
- [44] M. Abramowitz and I. A. Stegun, *Handbook of Mathematical Functions: With Formulas, Graphs, and Mathematical Tables* (Courier Corporation, 1965).
- [45] E. T. Whittaker and G. N. Watson, *A Course of Modern Analysis*, 4th ed., Cambridge Mathematical Library (Cambridge University Press, Cambridge, 1996).
- [46] M. K. Bin Subhan, A. Suleman, G. Moore, P. Phu, M. Hoesch, H. Kurebayashi, C. A. Howard, and S. R. Schofield, *Nano Letters* **21**, 5516 (2021).
- [47] P. Leininger, D. Chernyshov, A. Bosak, H. Berger, and D. S. Inosov, *Physical Review B* **83**, 233101 (2011).
- [48] Y. Tymoshenko, A.-A. Haghighirad, R. Heid, T. Lacmann, A. Ivashko, A. Merritt, X. Shen, M. Merz, G. Garbarino, L. Paolasini, A. Bosak, F. K. Diekmann, K. Rossnagel, S. Rosenkranz, A. H. Said, and F. Weber, *Communications Physics* **8**, 352 (2025).
- [49] J. Solyom, *Fundamentals of the Physics of Solids: Volume 3 - Normal, Broken-Symmetry, and Correlated Systems* (Springer, Berlin ; New York, 2010).
- [50] J. J. Sakurai and J. Napolitano, *Modern Quantum Mechanics* (Cambridge University Press, 2017).